Zulfah and Siripinyanond *Journal of Analytical Science and Technology* (2018) 9:19
https://doi.org/10.1186/s40543-018-0152-2

Journal of Analytical Science and Technology

RESEARCH ARTICLE Open Access

# Investigation of tin adsorption on silica nanoparticles by using flow field-flow fractionation with offline inductively coupled plasma mass spectrometry

Novy Lailatuz Zulfah and Atitaya Siripinyanond*

## Abstract

Flow field-flow fractionation (Fl-FFF) for silica nanoparticles with offline inductively coupled plasma mass spectrometry (ICP-MS) was applied to investigate the adsorption behavior of tin onto silica nanoparticles. Effect of carrier solutions and membranes was studied to achieve better separation for silica nanoparticles prior to tin detection using ICP-MS. Investigation was carried out by using 0.25 mM ammonium carbonate and 0.02% FL-70 with 0.02% $NaN_3$ as carrier solutions with 1 kDa regenerated cellulose (RC), 10 kDa regenerated cellulose (RC), and 10 kDa polyethersulfone (PES) membranes. Ammonium carbonate carrier solution with suitable ionic strength provided good separation with minimization of particle-membrane interaction. Better retention was shown by employing 10 kDa RC membrane. Furthermore, Fl-FFF was employed for the separation of silica nanoparticles incubated with tin. Fractions eluted from Fl-FFF were collected and then introduced into ICP-MS. Tin was adsorbed onto silica nanoparticles with different adsorption capabilities depending on particle size. Adsorption of tin was greater on the smaller size of silica nanoparticles compared to the bigger size with the adsorption percentage of 98.5, 44.9, and 6.5 for 60 nm, 100 nm, and 200 nm, respectively. Size-dependent adsorption of tin was in good agreement with surface area per volume of silica nanoparticles.

**Keywords:** Flow field-flow fractionation, Silica nanoparticles, Tin, Adsorption behavior, Inductively coupled plasma mass spectrometry

## Introduction

Synthetic nanosilica or silica nanoparticles have been used in diverse applications. They offer great stability with easy synthesis protocol (Rao et al. 2005). Synthetic silica nanoparticles are available in various forms such as powder, gel, precipitate, and colloid (Fruijtier-Polloth 2012). Addition of silica nanoparticles into dairy products provides the advantages of quality enhancement, such as to prevent caking and to act as thickening or emulsion stabilizer of some products such as coffee creamers, milk, soups, salts, sauces, and flours (Heroult et al. 2014). Silica nanoparticles with particle size of 30–200 nm were found in food products with concentration range of less than 0.1 to 6.9 mg $g^{-1}$ (Dekkers et al. 2011). The use of silica nanoparticles in food has attracted huge attention from researchers regarding their safety. Several potential toxicity risk investigations have been reported (Dekkers et al. 2011; van Kesteren et al. 2014; Peters et al. 2012). The presence of silica nanoparticles additive in food products changes the cell cycle of fibroblast cell in human which can undergo expression of stress reaction as well as antioxidant enzyme secretion (Athinarayanan et al. 2014).

Nowadays, food products are easily found as canned food. Canning process provides food preservation to extend the shelf life. Thin layer of tin or known as tinplate is coated inside the can body to enhance the robustness of food packaging. Tinplate minimizes the use of preservative due to the nature of tin as fungicide and bactericide. However, the use of tinplate triggers the dissolution of tin into foodstuff and exposing potential toxicity to consumers (Blunden and Wallace 2003). Several investigations have

* Correspondence: atitaya.sir@mahidol.ac.th
Department of Chemistry and Center for Innovation in Chemistry, Faculty of Science, Mahidol University, Rama VI Rd, Bangkok 10400, Thailand

noted that high level of inorganic tin contained in foods has possibility to trigger acute toxicity such as fever, headache, nausea, vomiting, diarrhea, bloating, and abdominal cramps. Concentration above 200 mg $kg^{-1}$ is known to provoke short-term effect as mentioned above (Perring and Basic-Dzorvak 2002). Moreover, storage condition of canned food, particularly the temperature, is predicted to have a non-trivial effect to the dissolution rate of tin. Dissolved tin from cans is likely bound to solid particles of food, and attachment of tin is known to be difficult to break (Weber 1987). In the presence of silica nanoparticles as food additive in canned food, dissolved tin would also be possible to bind onto silica nanoparticles. Several researchers have investigated the adsorption behavior of metal onto silica nanoparticles (Karnib et al. 2014; Ragab et al. 2017), and their adsorption of metal immensely enhanced the toxicity (Ragab et al. 2017). However, the adsorption behavior of tin onto silica nanoparticles has never been reported.

Assessment of adsorbed metal onto nanoparticles includes two steps, i.e., the separation of nanoparticles and the detection of metal residual by element determination techniques such as flame atomic absorption spectrometry (FAAS) or electrothermal atomic absorption spectrometry (ETAAS) (Karnib et al. 2014; Ragab et al. 2017). Field-flow fractionation (FFF) is a separation technique which has great ability for separating particles, molecules, and colloids in the range of nanometers up to micrometers. With FFF, various types of external field can be used, resulting in various FFF sub-techniques. Since flow field-flow fractionation (Fl-FFF) is known to provide excellent separation for many types of nanoparticles, it is interesting to explore the capability of Fl-FFF for this purpose. It is supported by many works that have successfully demonstrated separation, quantification, and characterization of silica nanoparticles (Dekkers et al. 2011; Grombe et al. 2014; Barahona et al. 2015; Aureli et al. 2015). Nonetheless, particles interaction with carrier solutions and accumulation wall under separation circumstance of Fl-FFF could not be neglected. Carrier solutions and membranes have critical influences to determine the quality of separation (Bendixena et al. 2014; Jochem et al. 2017; Benincasa and Caldwell 2001; Moon et al. 1998). Hence, the effects of carrier solutions and membranes for silica nanoparticles separation need to be examined.

Considering high dilution occurred during Fl-FFF separation, high sensitivity spectrometry technique needs to be employed for tin detection. Based on previous works for tin determination, inductively coupled plasma mass spectrometry (ICP-MS) revealed the highest sensitivity among spectrometry techniques (Knápek et al. 2009; Yuan et al. 2005; Trandafir et al. 2012). Therefore, in this study, Fl-FFF for silica nanoparticles with offline ICP-MS was employed to investigate adsorption behavior of tin onto silica nanoparticles. Effect of carrier solutions and membranes on the separation behavior of silica nanoparticles was also examined to achieve better separation.

## Methods

### Chemicals

Non-functionalized sphere silica nanoparticles (10 mg $mL^{-1}$) with the size of 60, 100, and 200 nm were purchased from Nanocomposix, Inc. (San Diego, CA, USA). FL-70 detergent (Fisher Chemical, Waltham, MA USA). Magnesium nitrate was bought from BDH VWR Analytical (Poole, England). Ammonium carbonate was purchased from Ajax Finechem (New South Wales, Australia). Tin dichloride was from Schalarau Chemie (Barcelona, Spain). Hydrochloric acid 37% was from ACI Labscan (Bangkok, Thailand). Sodium azide, sodium hydroxide, and palladium nitrate were bought from Merck (Darmstadt, Germany).

### Instrumentation

Symmetrical Fl-FFF equipped with flat rectangular separation channel with triangular endings was utilized. Mylar sheet spacer of 210-μm-thick was sandwiched between two plexiglass blocks with the ultrafiltration membrane placed on the top of the bottom block. UV-Visible detector Ver. 6.30 purchased from JASCO, Japan, was connected with Lab view software for data readout. Fl-FFF channel was connected to two HPLC pumps, which were channel flow pump model PN 1021 from Postnova Analytics (Landberg, Germany) and constametric III pump from Milton Roy (Houston, USA) for generating cross flow. Twenty microliters of sample was injected into the system through high-pressure injection valve. Three ultrafiltration membranes from Postnova Analytics were employed, which were 1 kDa regenerated cellulose (1 kDa RC), 10 kDa regenerated cellulose (10 kDa RC), and 10 kDa polyethersulfone (10 kDa PES). Aqueous solution of 0.02% (*v*/*v*) FL-70 with 0.02% (*w*/*v*) $NaN_3$ and ammonium carbonate 0.25 mM were utilized as carrier solutions. The fractograms were run for 30–40 min (depending on the particle size) and additional 15 min without cross flow applied after run for cleaning some particles which might be left on the accumulation wall. The optimized delay time (from the injection valve into separation channel) of 12 s was used to ensure that all particles had entered separation channel. The equilibrium time of 2 min was applied. The optimized channel flow rate and cross flow rate were chosen. Silica nanoparticles separation conditions are summarized in Table 1.

Fl-FFF system was coupled offline with inductively coupled plasma mass spectrometry (ICP-MS) model 7900 (Agilent Technologies, Santa Clara, CA, USA). The operating conditions of ICP-MS are listed in Table 2.

**Table 1** Fl-FFF operating conditions

| | |
|---|---|
| FFF channel dimensions (cm) | 28.7 cm long × 1.8 cm wide × 0.021 cm thick |
| Sample volume (μL) | 20 |
| Delay time (*s*) | 12 |
| Equilibrium time (min) | 2.0 |
| Membranes | 1 kDa RC, 10 kDa RC, 10 kDa PES |
| Carrier solutions | 0.02% (*v/v*) FL-70 with 0.02% (*w/v*) $NaN_3$, ammonium carbonate 0.25 mM |
| Channel flow rate (mL $min^{-1}$) | 1.0 |
| Cross flow rate (mL $min^{-1}$) | 0.8, 0.5[a] |

[a]This cross flow rate only applied in the use of 0.02% (*v/v*) FL-70 with 0.02% (*w/v*) $NaN_3$ carrier solution with 1 kDa RC

Hydrodynamic diameter of silica nanoparticles in different carrier solutions was determined by Zetasizer Nano-SZ from Malvern Instruments Ltd. (Malvern, UK).

The examination of silica nanoparticles contained in void fractions was carried out using transmission electron microscopy (TEM, JEM-1400HC, JEOL, Tokyo, Japan).

Moreover, scanning electron microscopy (SEM) model SU810 from Hitachi (Tokyo, Japan) was also used to find out membranes morphology in both surface mode and cross-section mode.

### Incubation of tin-silica nanoparticles

Interaction of tin-silica nanoparticles was investigated by incubation of silica nanoparticles in tin stock solutions, where 200 μL silica nanoparticles (10 mg $mL^{-1}$) was added into 40 μL of tin dichloride solutions (100 mg $L^{-1}$). Sonication was applied for 20 min, and the solution was left at room temperature for 24 h.

### Offline Fl-FFF with ICP-MS for silica nanoparticles

Silica nanoparticles were firstly incubated as mentioned above before introducing into the Fl-FFF system. The incubated silica was injected into Fl-FFF system by using the selected carrier solutions and membranes. Fractions from the separation peak were collected and diluted into the detectable range of ICP-MS. The diluted fractions were then subjected to ICP-MS detection.

**Table 2** ICP-MS operating condition for tin-silica nanoparticles investigation

| Agilent technologies 7900 ICP-MS | |
|---|---|
| Torch | Quartz with id of 2.5 mm |
| Monitored isotopes (m/z) | $^{118}Sn$, $^{120}Sn$ |
| Rf power (W) | 1500 |
| Rf matching (V) | 1.60 |
| Nebulizer gas flow (L $min^{-1}$) | 1.03 |
| Sample depth (mm) | 8.00 |
| Chamber temperature (°C) | 2 |

## Results and discussion

Silica nanoparticles were successfully separated by Fl-FFF with the use of two types of carrier solutions and different types of membranes. The elution order accordingly followed the Fl-FFF theory that 60 nm was eluted earlier than 100 nm and 200 nm, respectively. Distinct elution behavior of silica nanoparticles was obtained, as can be observed clearly from its retention time ($t_r$) (Table 3). Both membrane and carrier solution determine the separation performance inside the Fl-FFF channel. Particle-membrane interaction or particle-carrier interaction can cause changing of layer thickness toward the cross field applied and stream line toward the parabolic flow profile resulting in different retention times.

### Effect of membranes and carrier solutions on the separation behavior of silica nanoparticles

#### *Effect of membranes*

We examined three membranes with different types (regenerated cellulose and polyethersulfone) as well as different molecular weight cut-off (MWCO) (1 kDa and 10 kDa) with introduction of two types of carrier solutions including 0.02% (*v/v*) FL-70 with 0.02% $NaN_3$ (*w*/v) and 0.25 mM ammonium carbonate. Two types of membrane materials were examined, including regenerated cellulose and polyethersulfone as they are commercially available and commonly used in Fl-FFF separation. Although both membrane materials are hydrophilic, PES is more prone to hydrophobic interaction with particles coated with polymer. All membranes in this study have negative charges, which are suitable for separation of negatively charged silica particles, as the particle-membrane interaction is minimized. Silica nanoparticles behave differently when changing of membranes and carrier solutions as represented in the fractograms in Fig. 1. The higher separation peak height of silica nanoparticles was observed when using 10 kDa RC and 10 kDa PES membrane, as compared to that when using 1 kDa RC membrane. With the use of small MWCO membrane (1 kDa), large amount of particles were deposited in the vicinity of membrane during the equilibrium step then eluted as the peak after cross flow was terminated indicating the fouling of the membrane. The low retention with the use of 1 kDa RC is illustrated in Fig. 2. This finding could be explained by the electrolyte rejection mechanism as described by Mudalige et al., and the electrolyte rejection was influenced by MWCO of membrane (Mudalige et al. 2017). According to electrolyte rejection mechanism, negatively charged membranes rejected the anions of the electrolytes by electrostatic repulsion and retained the cations near the membrane surface, thereby electrolytes accumulated near the membrane. Membrane with smaller pores tends to have

**Table 3** Retention time of silica nanoparticles in various carrier solutions and membranes

| Particle size (nm) | Retention time (min) | | | | | |
|---|---|---|---|---|---|---|
| | Ammonium carbonate | | | FL-70 | | |
| | RC 1 kDa | RC 10 kDa | PES 10 kDa | RC 1 kDa | RC 10 kDa | PES 10 kDa |
| 60 | 4.06 | 3.86 | 5.10 | 5.56 | 5.93 | 5.80 |
| 100 | 7.31 | 7.01 | 7.39 | 9.36 | 9.55 | 7.63 |
| 200 | 15.89 | 17.31 | 17.74 | 16.80 | 22.78 | [a] |

[a]200 nm eluted under different optimum conditions

higher electrolyte rejection rate, because the greater electrostatic repulsion generated in between the pores and negative ions from the electrolyte conquered higher energy to get close on the membrane surface, and eventually, electrolyte concentration around the membrane was increased (Mudalige et al. 2017). In this case, the electrostatic repulsion from negatively charged silica nanoparticles and negatively charged membranes was suppressed due to the accumulated concentration of electrolyte near the membrane. It ultimately reduced membrane-particles distances and membrane fouling by silica nanoparticles. This membrane fouling effect could be more unsatisfactory in the presence of carrier solution with high ionic strength. As can be observed from the red line in Fig. 1a, FL-70 carrier solution showed poorer retention as compared to the red line in Fig. 1b.

Increasing the MWCO led to decreasing the void peaks, suggesting that membrane with larger MWCO performed better matrix removal efficiency (Kavurt et al. 2015). The void peak observed when using 1 kDa RC with 0.02% FL-70 with 0.02% $NaN_3$ carrier was very high as compared to the other two membranes. Void fractions of 100 nm and 200 nm silica nanoparticles were collected and introduced into TEM imaging for examination. We examined two zones in the TEM grid to get reliable results. Surprisingly, small number of silica nanoparticles was found in the collected fractions shown in Fig. 2. In void fraction of 100 nm, mean size of silica nanoparticles found was 86 nm and 92 nm for zone 1 and zone 2, respectively. For the void fraction of 200 nm, however, 178 nm was found in zone 1 and 83 nm found in zone 2. Regarding this finding, we

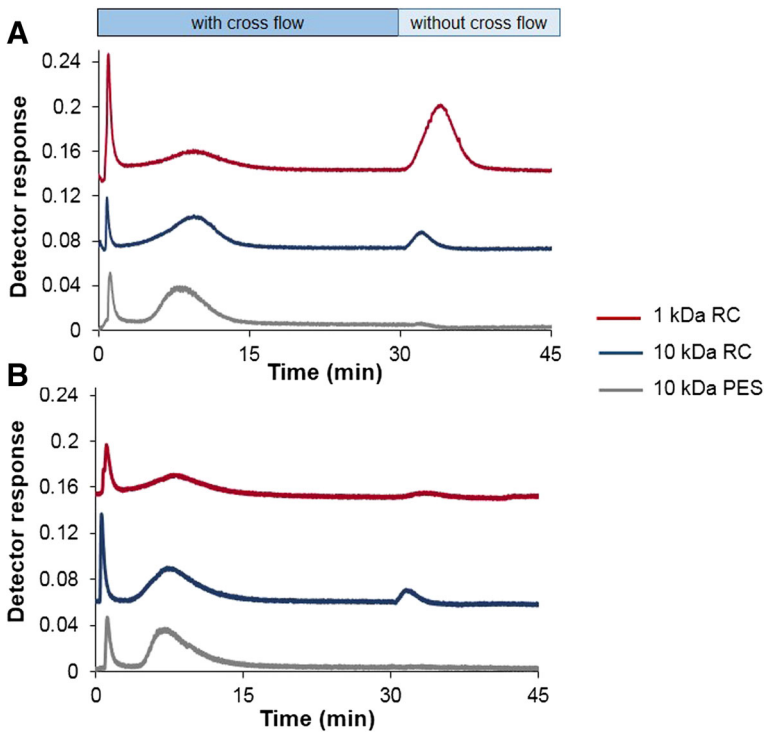


**Fig. 1** Comparison of peak appearance of 100 nm silica nanoparticles with various membranes: 1 kDa RC shown by red line, 10 kDa RC shown by blue line, and 10 kDa PES shown by gray line. Different carrier solutions were introduced: **a** 0.02% FL-70 with 0.02% $NaN_3$ and **b** 0.25 mM ammonium carbonate

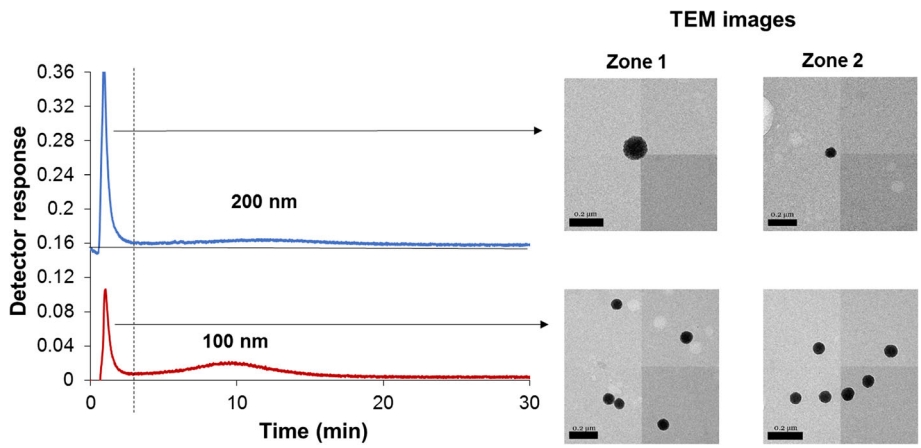


**Fig. 2** TEM images of the collected void fractions in use of RC 1 kDa obtained from the injection of silica nanoparticles 100 nm and 200 nm, with 0.02% FL-70 with 0.02% $NaN_3$ as carrier solutions. Zone 1 and zone 2 were from different area in TEM grid

speculate that in the presence of membrane fouling, the back pressure inside the channel was increased resulting in incomplete equilibrium occurred during relaxation step. Some of particles were deposited on the membrane causing membrane fouling, and some other particles nearer to injection port were not retained completely during the equilibrium time; therefore, some of particles were eluted as void fractions.

### *Effect of carrier solutions*

In this study, 0.02% (*v*/*v*) FL-70 with 0.02% $NaN_3$ (*w*/*v*) was used as carrier solution as normally used in Fl-FFF for nanoparticles separation including silica nanoparticles (Heroult et al. 2014; Aureli et al. 2015; Kato et al. 2018). As mentioned by Barahona et al. 2015, 0.25 mM ammonium carbonate offered good separation for silica nanoparticles (Barahona et al. 2015). Elution profiles of silica nanoparticles obtained from both carrier solutions are compared as shown in Fig. 3. The use of FL-70 with $NaN_3$ led to later elution as compared to silica nanoparticles eluted with ammonium carbonate as carrier solution. With the use of ammonium carbonate, the separation peak could be separated well from the void peak and well-defined separation peak was also observed. However, with FL-70, the nanoparticles were slowly eluted from the separation channel with strong retention.

Considering the retention time presented in Table 3, varying retention times from employing both of carrier solutions could depict the different carrier properties acting to the silica nanoparticles. Ammonium carbonate is the volatile buffer, whereby FL-70 with $NaN_3$ is the mixture between complex surfactant and inorganic salt. The prominent property which distinguishes those carrier solutions is ionic strength. In the presence of sodium azide, the ionic strength of FL-70 with $NaN_3$ is a lot higher than that of ammonium carbonate with ionic strength of 3.24 mM and 0.75 mM, respectively (Table 4). The retention is typically sensitive to the content of sodium salt (Benincasa and Caldwell 2001). Recently, Kato et al. described that Debye length was minimized in the increasing of electrolyte molecules (Kato et al. 2018). Higher ionic strength carrier induced the reduction of electrostatic interactions between the silica nanoparticles yet resulting in higher attractive interaction between silica nanoparticles and the membrane, making the longer retention time (Barahona et al. 2015). A small peak was observed after stopping cross flow indicating that some amounts of silica nanoparticles strongly retained close to the membrane surface and could not be eluted in the separation step in case of FL-70 with $NaN_3$. Strong interaction between membrane and particles led to inaccurate particle information. On the other hand, in the suitable ionic strength which is ammonium carbonate in

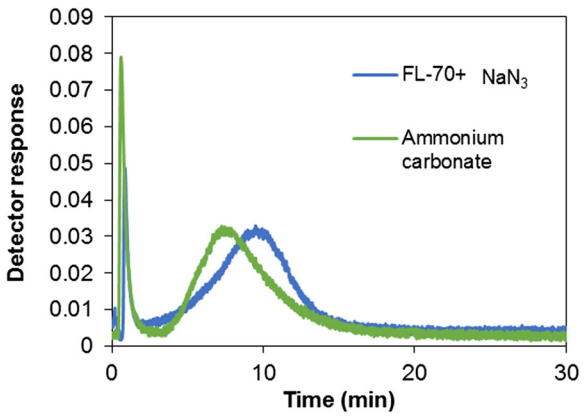


**Fig. 3** Comparison of elution profiles of 100 nm silica nanoparticles with 0.02% FL-70 with 0.02% $NaN_3$ (blue) and 0.25 mM ammonium carbonate (green) as carrier solutions, with the use of membrane RC 1 kDa

**Table 4** Properties of carrier solutions

| Carrier solutions | 0.02% (*v/v*) FL-70 with 0.02% (*w/v*) $NaN_3$ | 0.25 mM ammonium carbonate |
|---|---|---|
| Type of chemical | Surfactant with inorganic salt | Buffer |
| pH | 8.9 | 7.6 |
| Ionic strength (mM) | 3.24 | 0.75 |

this study (lower ionic strength than FL-70 with $NaN_3$), silica nanoparticles exhibited lower attractive interaction with membrane as it was evidenced by the observation that no peak was found after stopping the cross flow. Moreover, the controlled pH of this carrier (pH 9) is suitable for the stability of silica nanoparticles (Barahona et al. 2015). Appropriate carrier solution with minimum interaction should be chosen to give reliable information of nanoparticles regarding with their hydrodynamic size. Apart from some reasons mentioned earlier, ammonium carbonate carrier solution was preferable to use for further experiment with offline coupling ICP-MS. Its volatility is known to provide better background signal, minimize contamination, and prevent the interference under instrumentation set up of ICP-MS (Barahona et al. 2015).

#### *Relative fractionation recovery*

Fractionation recovery is a very important parameter to consider for the quantitative analysis in Fl-FFF technique. All parameters mentioned above importantly contribute to the relative fractionation recovery of silica nanoparticles as observed in Fig. 4. Fractionation recovery controls the quantitative analysis particularly in Fl-FFF technique. Relative fractionation recovery is calculated by dividing the peak area obtained from injection with applying cross flow ($S$) to the peak area obtained from the injection without cross flow applied ($S_0$) as expressed in the following equation (Bolea et al. 2011):

$$R\,(\%) = \frac{S}{S_0} \mathrm{x}\ 100$$

Percentage of recovery decreased along with increasing the particle size in the case of 1 kDa RC, in the case10 kDa RC with ammonium carbonate carrier (Fig. 4b), and in the case of 1 kDa RC and 10 kDa PES with FL-70 with $NaN_3$ carrier (Fig. 4a). Opposite trend was shown by 10 kDa RC with FL-70 with $NaN_3$ carrier that the percentage of recovery increased with increasing particles size. For 10 kDa PES with ammonium carbonate carrier, the percentage of recovery was similar to all particle sizes studied herein. With the smallest MWCO of membrane, lower retention of silica nanoparticles (smaller separation peak height) in both of carrier solutions was observed. This effect will be worse for larger size of nanoparticles as they have lower self-diffusion, so they are prone to stay closer to the membrane, as the result poor recovery was shown for 200 nm. Both carriers provided desirable recoveries with negligible difference in case of 10 kDa membranes. Considering the excellent percentage of relative recovery obtained, 10 kDa RC was considered for further experiment.

### Investigation of tin adsorption onto silica nanoparticles by Fl-FFF with offline ICP-MS

Silica nanoparticles incubated in tin standard solution were introduced into Fl-FFF system using 0.25 mM ammonium carbonate as carrier solution and 10 kDa RC membrane. Different sizes of silica nanoparticles were incubated with tin in order to investigate particle size effect related with their adsorption efficiency toward tin. The incubated mixture solution was directly introduced into an Fl-FFF channel without any extra separation step. The Fl-FFF separation condition for the tin-adsorbed silica nanoparticles was modified from that used for bare silica nanoparticles due to slower elution observed by the shift of peak to the longer time for the core silica particles of the same size. Prominent band broadening was also noticed, and it made particles eluted in longer time. This observation leads to our hypothesis that aggregation of silica nanoparticles was triggered by the presence of tin. Considering that tin standard has pH close to pH 2, it rendered the mixture between tin and silica nanoparticles to approximately pH 2. Aggregation of silica nanoparticles might happen in the pH of 2 or lower because at that pH range, silica nanoparticles reach isoelectric point. At the isoelectric point, the zeta potential of silica nanoparticles is close to zero or very low which means that the nanoparticles are electrically unstable. Therefore, nanoparticles tend to aggregate. Decreasing applied cross flow rate did not help to improve the separation. Improvement of separation was achieved by applying higher channel flow rate and shortening relaxation time. With shorter relaxation time, particles were expected to have shorter time to interact with membrane as they were forced by cross flow in the shorter time. As a result, band broadening could be minimized. Shift in retention time was observed in all sizes of silica nanoparticles in the presence of tin as compared to retention time of bare silica nanoparticles, as shown in Fig. 5. Retention time shift was greater in smaller size and decreased in increasing of particles size. Further investigation is needed to explain this phenomenon in more details.

Fractions of silica nanoparticles were collected from the time when the peak started to show up until the peak reached the baseline. Collected fractions were then adjusted to the volume and introduced into ICP-MS system with operating conditions listed in Table 2. Tin standard solutions with the concentration ranging from 0.5–10.0 μg $L^{-1}$ were

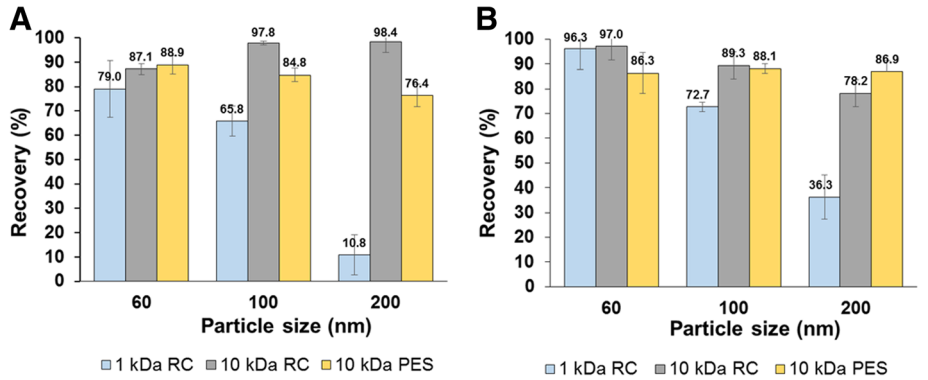


**Fig. 4** Relative fractionation recovery of 60, 100, and 200 nm of silica nanoparticles obtained with the use of various membranes: 1 kDa RC (blue), 10 kDa RC and (gray), and PES 10 kDa (yellow) in different carrier solutions. **a** 0.02% FL-70 with 0.02% $NaN_3$ and **b** 0.25 mM ammonium carbonate

introduced to construct calibration curve prior to fractions analysis. Calibration curve was constructed to perform the quantification of tin adsorbed onto silica nanoparticles. According to the work from Yu in 2010, $^{118}Sn$ and $^{120}Sn$ showed highest abundances and are less disturbed by oxides (Yu et al. 2010). Therefore, two tin isotopes were monitored in this work. $^{120}Sn$ showed great linear relationship between intensity and tin concentration with the relation coefficient of 0.9984. Tin was found in the collected fractions suggesting that tin could be bound onto silica nanoparticles. Electrostatic interaction and strong coordinate bonds between adsorbed tin ions with weak acidity of hydroxyl from silanol groups on silica nanoparticles surface has known to be suitable adsorption mechanism (Ragab et al. 2017). Carrier solution flow did not ruin the interaction between tin with silica nanoparticles as we could see tin intensity in the collected fractions. It is interesting to note that the application of Fl-FFF with offline ICP-MS could be applied for investigation of adsorption behavior of tin onto silica nanoparticles.

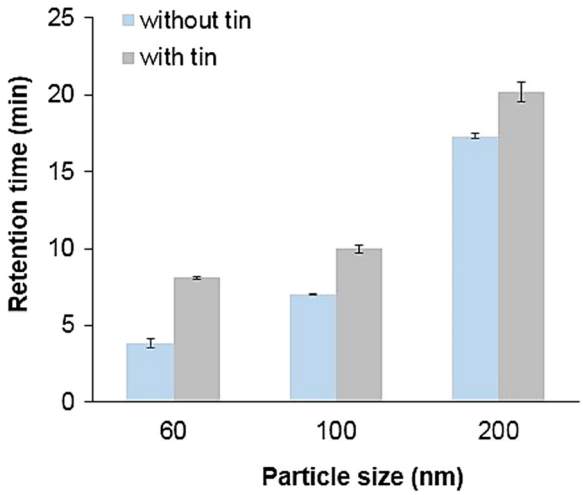


**Fig. 5** The relationships between the retention time (*y*-axis) and particle size (*x*-axis) of different-sized silica nanoparticles in the absence of tin and incubated in tin. The fractionation was carried out using 0.25 mM ammonium carbonate and 10 kDa RC as carrier solution and membrane, respectively

### *Effect of silica nanoparticles size on tin adsorption*

According to the results, tin intensity from fractions was influenced by size of silica nanoparticles. Decreasing tin intensity was observed along with increasing particle size. Tin adsorbed onto different-sized silica nanoparticles was further determined. It was known that amount of adsorbed tin increased with the decreasing size of silica nanoparticles. Percentage of tin adsorption onto silica nanoparticles was calculated using the equation:

$$\%\text{adsorption} = \frac{\text{amount of tin found in silica nanoparticles}}{\text{initial amount of tin}} \text{ x } 100$$

The percentage of adsorption is greatest for 60 nm of silica nanoparticles as shown in Table 5. Increasing particle size leads to lowering tin adsorption. Significant reduction of tin adsorption was shown by the largest size which is 200 nm. Surface area of silica nanoparticles was expected to explain this finding. In this case, surface area was calculated as total surface area of silica nanoparticles. The total surface area was calculated based on the amount of particles in the certain volume of incubated

**Table 5** Percentage of tin in different-sized silica nanoparticles

| Sample | % adsorption | RSD |
|---|---|---|
| Fraction 60 nm | 98.5 | 1.2 |
| Fraction 100 nm | 44.9 | 3.6 |
| Fraction 200 nm | 6.5 | 9.0 |

silica. By calculating total surface area of incubated silica nanoparticles, silica nanoparticles with the size of 60 nm show largest surface area per volume followed by 100 nm and 200 nm, respectively. The relationship between surface areas of incubated silica nanoparticles was plotted with the percentage of tin adsorbed as illustrated in Fig. 6. Size dependence adsorption capability of silica nanoparticles toward tin was observed in this work. Adsorption of tin was controlled by surface area of silica nanoparticles which is related with their particles size. Surface area increased along with decreasing particles size, as the result adsorption of tin was greater in smaller size. This is related with the shift of retention time from the Fl-FFF result for bare silica nanoparticles by which the smaller particles showed larger shift in retention time. Smaller particles were proven to adsorb more tin as the result the aggregation was increased and eluted in later time. In order to obtain the optimum adsorption efficiency, knowing size information of silica nanoparticles is essential. Based on the works of some researchers, Fl-FFF could provide size information and quantification of silica nanoparticles (Barahona et al. 2015). From this finding, it is demonstrated that Fl-FFF also offers powerful separation of silica nanoparticles as tin adsorbent prior to tin analysis. Therefore, it could be beneficial for employing Fl-FFF in the determination of adsorption behavior of tin onto silica nanoparticles.

## Conclusions

Adsorption behavior of tin onto nanoparticles was investigated by Fl-FFF with offline ICP-MS. Fl-FFF was employed for the separation of silica nanoparticles incubated with tin prior to the tin analysis by ICP-MS. Solid particles could be excluded from supernatant and accumulated as eluted fractions. Collected fractions were introduced into ICP-MS for tin detection. Effect of carrier solution and membranes was firstly investigated to obtain desired separation of silica nanoparticles. Ionic strength of carrier solution was considered. The nature of ammonium carbonate offers beneficial for both Fl-FFF and ICP-MS systems. Separation performance was also affected by MWCO and material of the membrane. Adsorption of tin onto silica nanoparticles depended on the size of silica nanoparticles. Tin adsorption was increased in the decreasing of particles size as their surface area per volume increased along with decreasing particles size. The order of tin adsorption capability of silica nanoparticles from the greatest to the least are 60 nm, 100 nm, and 200 nm, respectively. The size differentiation of silica nanoparticles was important. The advantages of using Fl-FFF in this work were emphasized by performing separation as well as giving size information of silica nanoparticles.

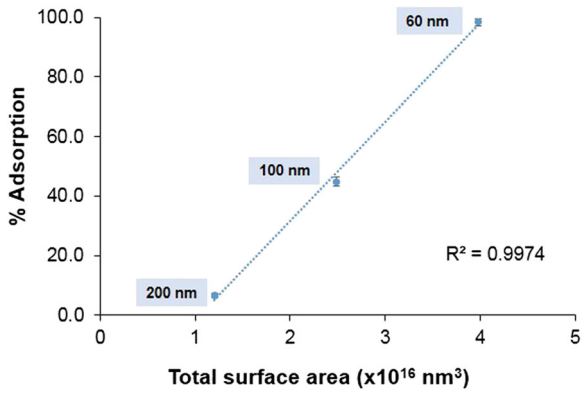


**Fig. 6** Plot of adsorption percentage of tin onto silica nanoparticles and total surface area of incubated silica nanoparticles. Adsorption behavior of tin was determined by size of silica nanoparticles. Surface area increased along with decreasing nanoparticles size

**Acknowledgements**
We sincerely acknowledge the research grant from Center for Innovation in Chemistry: Postgraduate Education and Research Program in Chemistry (PERCH-CIC) in collaboration with National Research Council of Thailand (NRCT) and International Foundation for Science (IFS). Thanks are also due to Thailand Research Fund (TRF) and Mahidol University for providing the research grant under the grant number BRG6180006. Funding from the Thailand Research Fund under the grant number IRN59W0007 is also acknowledged. We would like to thank Dr. Ronald G. Beckett for donating some parts of FIFFF system.

**Authors' contributions**
NLZ performed all the experimental works. AS coordinated and planned the work. All authors read and approved the final manuscript.

**Ethics approval and consent to participate**
Not applicable

**Consent for publication**
Not applicable

**Competing interests**
The authors declare that they have no competing interests.

## Publisher's Note



Received: 8 July 2018 Accepted: 7 September 2018
Published online: 18 September 2018

**References**

Athinarayanan J, Periasamy VS, Alsaif MA, Al-Warthan AA, Alshatwi AA. Presence of nanosilica (E551) in commercial food products: TNF-mediated oxidative stress and altered cell cycle progression in human lung fibroblast cells. Cell Biol Toxicol. 2014;30:89–100.

Aureli F, D'Atmo M, Raggi A, Cubadda F. Quantitative characterization of silica nanoparticles by asymmetric flow field flow fractionation coupled with online multi angle light scattering and ICP-MS/MS detection. J Anal At Spectrom. 2015;30:1266–73.

Barahona F, Geiss O, Urbán P, Ojea-Jimenez I, Gilliland D, Barrero-Moreno J. Simultaneous determination of size and quantification of silica nanoparticles by asymmetric flow field-flow fractionation coupled to ICPMS using silica nanoparticles standards. Anal Chem. 2015;87:3039–47.

Bendixena N, Loserta S, Adlhart C, Lattuada M, Ulrich A. Membrane–particle interactions in an asymmetric flow field flow fractionation channel studied with titanium dioxide nanoparticles. J Chromatogr A. 2014;1334:92–100.

Benincasa MA, Caldwell KD. Flow field-flow fractionation of poly(ethylene oxide): effect of carrier ionic strength and composition. J Chromatogr A. 2001;925:159–69.
Blunden S, Wallace T. Tin in canned food: a review and understanding of occurrence and effect. Food Chem Toxicol. 2003;41:1651–62.
Bolea E, Jiménez-Lamana J, Laborda F, Castillo JR. Size characterization and quantification of silver nanoparticles by asymmetric flow field-flow fractionation coupled with inductively coupled plasma mass spectrometry. Anal Bioanal Chem. 2011;401:2723–32.
Dekkers S, Krystek P, Peters JB, Lankveld DPK, Bokkers BGH, van Hoeven-Arentzen PH, Bouwmeester H, Oomen AG. Presence and risks of nanosilica in food products. Nanotoxicol. 2011;5:393–405.
Fruijtier-Polloth C. The toxicological mode of action and the safety of synthetic amorphous silica—a nanostructured material. Toxicology. 2012;294:61–79.
Grombe R, Charout-Got J, Emteborg H, Linsinger TPJ, Seghers J, Wagner S, von der Kammer F, Hofmann T, Dudkiewicz A, Llinas M, Solans C, Lehner A, Allmaier G. Production of reference materials for the detection and size determination of silica nanoparticles in tomato soup. Anal Bioanal Chem. 2014;406:3895–907.
Herault J, Nischwitz V, Bartczak D, Goenaga-Infante H. The potential of asymmetric flow field-flow fractionation hyphenated to multiple detectors for the quantification and size estimation of silica nanoparticles in a food matrix. Anal Bioanal Chem. 2014;406:3919–27.
Jochem A–R, Ankah GN, Meyer L–A, Elsenberg S, Johann C, Kraus T. Colloidal mechanisms of gold nanoparticle loss in asymmetric flow field-flow fractionation. Anal Chem. 2017;88:10065-–10073.
Karnib M, Kabbani A, Holaila H, Olamaa Z. Heavy metals removal using activated carbon, silica and silica activated carbon composite. Energy Procedia. 2014;50:113–20.
Kato H, Nakamura A, Banno H, Shimizu M. Separation of different-sized silica nanoparticles using asymmetric flow field-flow fractionation by control of the Debye length of the particles with the addition of electrolyte molecules. Colloid Surf A. 2018;538:678–85.
Kavurt UB, Marioli M, Kok WT, Stamatialis D. Membranes for separation of biomacromolecules and bioparticles via flow field-flow fractionation. J Chem Technol Biotechnol. 2015;90:11–8.
Knápek J, Herman V, Buch tová R, Vošmerová D. Determination of tin in canned foods by atomic absorption spectrometry. Czech J Food Sci. 2009;27:S407–9.
Moon MH, Park I, Kim Y. Size characterization of liposomes by flow field-flow fractionation and photon correlation spectroscopy: effect of ionic strength and pH of carrier solutions. J Chromatogr A. 1998;813:91–100.
Mudalige TK, Qu H, Linder SW. Flow field-flow fractionation: effects of membrane molecular weight cut-off size, fluid dynamics and valence of electrolytes. Langmuir. 2017;33:1442–50.
Perring L, Basic-Dzorvak M. Determination of total tin in canned food using inductively coupled plasma atomic emission spectroscopy. Anal Bioanal Chem. 2002;374:235–43.
Peters R, Kramer E, Oomen AG, Rivera ZEH, Oegema G, Tromp PC, Fokkink R, Rietveld A, Marvin HJP, Weigel S, Peijnenburg AACM, Bouwmeester H. Presence of nano-sized silica during in vitro digestion of foods containing silica as a food additive. ACS Nano. 2012;6:2441–51.
Ragab MAA, Korany MA, Ibrahim HZ, Abdel-Kawi MA, Sayed AEAAA. Adsorption behavior of some metal ions on nanoparticles used in pharmaceutical matrices: application to laboratory made drug formulation. Bull Fac Pharm (Cairo Univ). 2017;55:155–62.
Rao KS, El-Hami K, Kodaki T, Matsushige K, Makino K. A novel method for synthesis of silica nanoparticles. J Colloid Interface Sci. 2005;289:125–31.
Trandafir I, Nour V, Ionica ME. Determination of tin in canned food by inductively coupled plasma-mass spectrometry. Pol J Environ Stud. 2012;21:749–54.
van Kesteren PCE, Cubadda F, Bouwmeester H, van Eijkeren JCH, Dekkers S, de Jong WH, Oome AG. Novel insights into the risk assessment of the nanomaterial synthetic amorphous silica, additive E551, in food. Nanotoxicol. 2014;9:442–52.
Weber G. Speciation of tin in lemon juice: an example of trace metal speciation in food. Anal Chim Acta. 1987;200:79–88.
Yu Z–H, Sun J–Q, Jing M, Cao X, Lee F, Wang X–R. Determination of total tin and organotin compounds in shellfish by ICP-MS. Food Chem. 2010;119:364–7.
Yuan C–G, Jiang G–B, He B, Liu B-F. Preconcentration and determination of tin in water samples by using cloud point extraction and graphite furnace atomic absorption spectrometry. Microchim Acta. 2005;150:329–34.